2020 IEEE International Conference on Robotics and Automation (ICRA)
31 May - 31 August, 2020. Paris, France

Collaborative Robot-Assisted Endovascular Catheterization with Generative Adversarial Imitation Learning

Wenqiang Chi[1], Giulio Dagnino[1], Trevor M. Y. Kwok[2], Anh Nguyen[1], Dennis Kundrat[1], Mohamed E. M. K. Abdelaziz[1], Celia Riga[2], Colin Bicknell[2] and Guang-Zhong Yang[3], *Fellow*, *IEEE*

***Abstract*— Master-slave systems for endovascular catheterization have brought major clinical benefits including reduced radiation doses to the operators, improved precision and stability of the instruments, as well as reduced procedural duration. Emerging deep reinforcement learning (RL) technologies could potentially automate more complex endovascular tasks with enhanced success rates, more consistent motion and reduced fatigue and cognitive workload of the operators. However, the complexity of the pulsatile flows within the vasculature and non-linear behavior of the instruments hinder the use of model-based approaches for RL. This paper describes model-free generative adversarial imitation learning to automate a standard arterial catherization task. The automation policies have been trained in a pre-clinical setting. Detailed validation results show high success rates after skill transfer to a different vascular anatomical model. The quality of the catheter motions also shows less mean and maximum contact forces compared to manual-based approaches.**

I. INTRODUCTION

Endovascular intervention is increasingly adopted for the treatment of various types of cardiovascular disease, which is the major cause of death in the Western world [1]. Catheterization is the key technical component of these interventions: surgeons manipulate pre-shaped instruments such as catheters and guidewires to reach the target vasculature, enabling delivery of treatments such as stenting, embolization and drugs. However, catheterization requires complex maneuvers of elongated instruments; experience and skill are crucial to the success of the procedure. Moreover, the lack of 3D imaging for visualizing the tissue also presents further difficulties. As these procedures are performed with X-ray fluoroscopic guidance, both patients and operators are exposed to radiation and its associated health risks. Potential risks of instrument manipulation within blood vessels include tissue dissection, thrombosis, and embolization [2].

In order to address the aforementioned challenges, commercial robotic systems for endovascular intervention have been developed. The *Magellan* system (Auris Health, Redwood city, CA, USA) features proprietary steerable catheters with enhanced maneuverability and stability. Other commercial platforms focus on remote control of off-the-shelf catheters and guidewires, such as the *CorPath*® GRX system (Corindus Vascular Robotics, MA, USA) and the *R-one*™ robot (Robocath, Rouen, France). These robotic platforms offer reduced X-ray exposure to operators, and increase the accuracy of the procedure, allowing precise control of the instruments while reducing the cognitive workloads of the operators [3]. However, one shortcoming of these platforms is the suboptimal ergonomic design of the user interface. The use of multiple Degree-of-Freedom (DoF) haptic devices and buttons results in significant change of the behavioral patterns when compared to that of manipulating conventional endovascular instruments. Therefore, many research platforms were designed to utilize natural catheter/guidewire manipulation with ergonomic master devices [4], [5], [6].

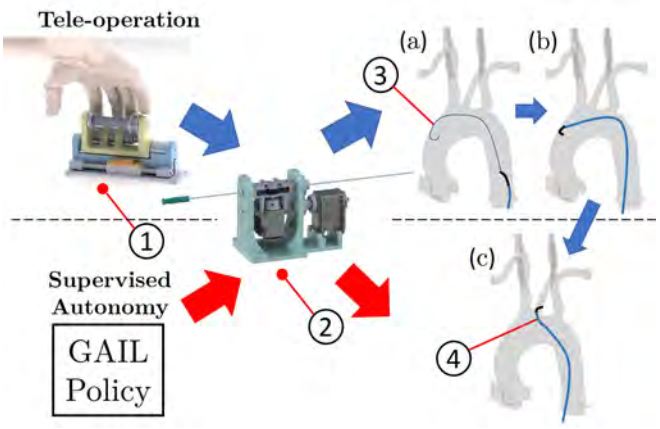

Fig. 1: The proposed shared autonomy scenario. **Human phase:** (a) The guidewire is manually pre-loaded; (b) The catheter was inserted by the operator using the master-slave robotic system. **Supervised autonomy phase:** (c) The robot automatically cannulates to the branch vessel under supervision of the surgeon. Annotation: (1) robotic master manipulator. (2) robotic catheter manipulator. (3) guidewire, and (4) blue part:catheter body; black part: pre-shaped tip.

In general, those robotic platforms offer low levels of robotic autonomy [7] and the majority follow the master-slave paradigm for instrument teleoperation. Surgical autonomy has attracted much attention in recent years. Its potential advantages include reduced fatigue for clinicians, lower rates of human error, faster integration of context-aware information such as medical imaging and physiological signals, as well as increased accuracy of instrument manipulation [8]. However, as fully automated surgery is a long way from becoming a reality, operator-centric and shared control frameworks are more practical approaches to combine machine precision and human intelligence. In the field of

[1]Hamlyn Centre, Imperial College London, SW7 2AZ, London, UK (email:wenqiang.chi10@imperial.ac.uk)
[2] Department of Surgery and Cancer, Imperial College London, St Mary's Hospital, W2 1NY, London, UK
[3] Institute of Medical Robotics, Shanghai Jiao Tong University, Shanghai, China

endovascular intervention, Corindus has received Food and Drug Administration (FDA) clearance for the first automated robotic movement in its *CorPath*® GRX system, with which manipulation of the guidewire is partially automated in response to the operators' actions. In [9], the authors claim that the automation feature offers shorter catheterization times and enhanced precision. Several research efforts to semi-automate catheterization showed promising results in improved quality and safety of the procedure [10], [11], [12], [13], and reduced procedural and radiation time [10].

Emerging development of deep reinforcement learning (RL) has facilitated task autonomy for robotics in general, including Alpha Go that can perform self-optimization of game policies without any expert demonstration [14]. Recent advances in deep RL have resulted in an ability to perform imitation learning purely based on human demonstration with unknown dynamics of the environment [15], which is useful for tasks that require complex skills in a dynamic environment, for example, surgical tasks in dynamic anatomies. Such imitation learning frameworks have been successfully demonstrated to perform real-world tasks by robotic systems, such as navigation, locomotion and object manipulation [16], [17], [18]. It also has been used for skill training of minimally invasive surgery [19]. The level of surgical autonomy can potentially shift towards task autonomy with the input from deep RL, where the robot can take over part of the decision making when executing a surgical task under human supervision [7].

In this paper, a collaborative robot-assisted endovascular catheterization framework is proposed. An example clinical scenario is illustrated in Fig. 1, where a human operator has advanced an angiographic catheter to the ascending aorta with the CathBot platform [4]. At this stage the proposed automation system will take over the control of the robotic catheter manipulator to cannulate the target branch artery of the aorta. A model-free generative adversarial imitation learning (GAIL) method was implemented to acquire a catheterization technique from multiple demonstrations by an expert vascular surgeon. The catheterization policies were trained in the real world with a pre-clinical setting that facilitates *in-vivo* implementation. Our approaches successfully imitate the task with unknown dynamics of simulated blood flows, tissue-tool interactions and the flexible instruments.

It is important to establish the distinction between the work presented in this paper and the previous work of the authors. The current framework has closed-loop control of the robot, where the robot executes action trajectories taking into account to the position and orientation of the catheter within the vasculature. For this, an electromagnetic (EM) tracking sensor is attached to the tip of the catheter, which has been used for automation and navigation of endovascular catheterization in pre-clinicial settings [10]. In contrast, [12] and [13] described execution of preprogrammed robotic trajectories without perceiving the state of the task. Hence the proposed approach has greater adaptation to different initial conditions and dynamic environment when collaborating with a human operator. Moreover, the proposed

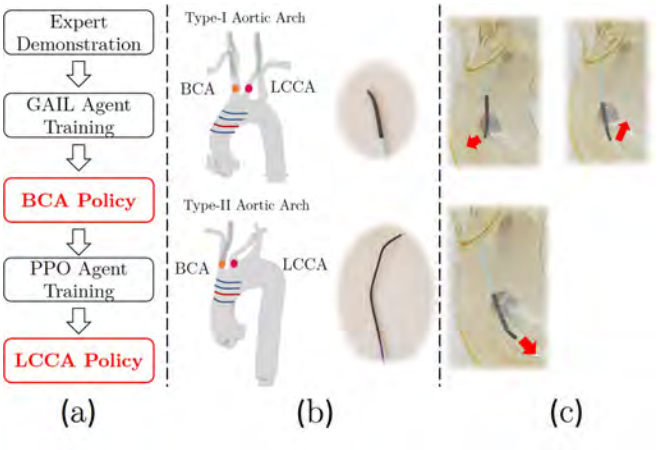

Fig. 2: (a) Overview of the proposed imitation learning strategy. (b) **Left:** Orange points: the target, 5mm upper to the origin of BCA; Red points: the target, 5mm upper to the origin of LCCA; Colored bands: the starting positions of the catheter in the training phase, red bands: the starting positions for the user studies. **Right:** A VanSchie2 catheter (top). A Headhunter1 catheter (bottom). (c) Three different angles where the catheter tip is pointing to.

imitation learning extracts the latent skills from the expert demonstration and are transferable to different catheters, anatomies and flow conditions with a relatively small amount of demonstration data.

II. Materials and Methods

This section includes the methodologies for expert demonstration collection and motion segmentation, the GAIL and Proximal Policy Optimization (PPO) agents training (was originally introduced in [21]), and the experiments.

A. Task Demonstration

To obtain training sets for the proposed imitation learning approach, an expert surgeon ($>$ 700 cases) performed a selective catheterization task (8 times) to the brachiocephalic artery (BCA) (Fig. 2(b)), using the CathBot system in a silicone-based, transparent, anthropomorphic phantom, of a Type-I aortic arch model (Elastrat Sarl, Switzerland). A catheter (Beacon Tip 5 Fr VanSchie2, Cook Medical, Bloomington, IN) was used in the task. The CathBot system, introduced in [4], is a robotic platform featuring a master manipulator (Fig. 3) that mimics and maps the natural manual intra-procedural handling of standard catheters and guidewires. Hence the maneuvers and the skills of the surgeon can be preserved. The catheter is driven by a robotic slave manipulator (Fig. 3) that has been introduced in [11].

Selective Catheterization: The task to be automated was selective catheterization of, or advancement of an angiographic catheter into, the 2 major branches of the aortic arch, namely the brachiocephalic artery (BCA) and left common carotid artery (LCCA). This was to be achieved with the catheter having been advanced retrograde from the descending thoracic aorta, which is generally the case in real clinical situations. For the task, the starting position of the

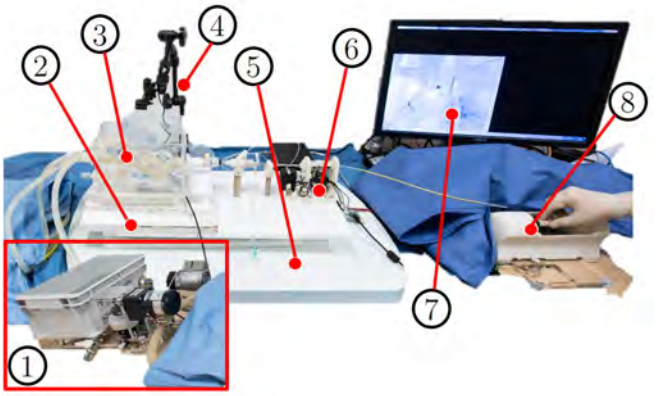

Fig. 3: Experimental setup of the proposed robotic platform: (1) Pulsatile and continuous flow pumps, (2) Force Sensor, (3) Vascular phantom, (4) Webcam, (5) NDI Aurora field generator, (6) Catheter manipulator, (7) Simulated X-ray Screening, and (8) Master device.

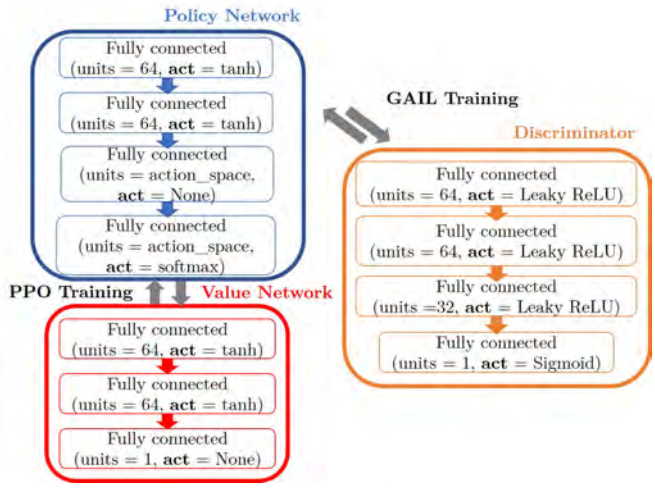

Fig. 4: Overview of the proposed GAIL and PPO agents training architecture. **"act"** is the abbreviation of word "activation".

catheter tip was defined at a position in the aorta beyond (proximal to) the major branches.

Motion Signal Collection: Catheter tip pose (position and rotation) and CathBot manipulator linear/rotary motions were recorded during the catherization tasks. A six DoF EM tracking sensor (Aurora, NDI) was attached to the tip of the catheter. Velocities of the linear and rotary motors of the manipulator were acquired, and synchronized with the catheter pose provided by the EM tracking system. Rigid point set registration between the EM tracking system and the CT scan of the vascular phantom is performed using CT markers. Therefore, mapping between catheter tip poses with respect to the registered anatomy can be calculated.

State-Action Pair Segmentation: The operator's hand motions are defined as five motion primitives, which are: 1) push; 2) pull; 2) rotation clockwisely; 4) rotation anti-clockwisely; 5) stand-by. Due to the damping forces caused by the motors in the master device, we observed nearly constant speed when the operator is using the device. For simplification, we assumed constant speed for each action taken by the operator. The velocities of the linear and angular motions were averaged accordingly as $\mathbf{v}$ and ω, so the action set $\{a\} = \{\mathbf{v}, -\mathbf{v}, \omega, -\omega, 0\}$, information of tip of the catheter is $s_t = (x_t, y_t, z_t, \sigma_x, \sigma_y, \sigma_z)$, where the first three components represent the positions of the tip while the rest represents the Euler angles of the EM sensor with respect to frame of the field generator. Manual discretization is performed to segment the motion trajectories into state-action pairs, based on the average time taken to complete a translational or rotational movement. Anatomical information is integrated into the training sets, relative positions of the catheter tip to the target vessels are calculated. This is done by subtracting a reference point at the blood vessel, which is the central point at the origin of the BCA (Fig. 2(b)).

B. GAIL and PPO Agents Training

The policy for cannulation to BCA are generated from GAIL agents training. The main objective of the training is to extract underlying motion patterns from expert demonstration. GAIL is a model-free algorithm for imitation learning [15], which is suitable in the catheterization task where the dynamics of both the vasculature and the flexible instruments are complex. Compared to the traditional inverse optimal control approach [20], GAIL directly generates policies instead of reward functions, which is much simpler to be implemented by robotic systems. The principle of GAIL is inspired by the Generative Adversarial Networks (GAN), which consists of a discriminator D_w and a policy generator $G_{w'}$, where w denotes the parameters associated with each network. The policy network generates exploration trajectories which are used by the discriminator to separate the generator policy from the expert policy. The discriminator is trained to minimize the loss function:

$$L^D = \mathbb{E}_{\tau_i}[\log(D_w(s_t,a))] + \mathbb{E}_{\tau_E}[\log(1 - D_w(s_t,a))] \qquad (1)$$

where τ_i are the trajectories generated by $G_{w'}$ and τ_E are the expert trajectories. The policy generator $G_{w'}$ is trained by PPO which consists of a policy network and a value network; the update rule can be found in [21].

The GAIL agents are trained directly in real-world with the CathBot system in a pre-clinical setting, the protocol is similar to previous work [13]. The setup contains soft vascular phantoms, blood flow simulation, and off-the-shelf surgical instruments (Beacon Tip 5 Fr VanSchie2, Cook Medical, Bloomington, IN), as shown in Fig. 3. Compared to training in virtual simulation platform, our approach facilitates the implementation of the learned policies to real robotic systems. For one training rollout, the state s_t is recorded from the EM tracking system, then the relative position of the tip to the origin of the target vessel is calculated, hence target vessel can be changed by substituting the origin. The action is generated by the policy generator $G_{w'}$, it is then executed by the slave robot with velocities of $\mathbf{v}$ and ω, the on/off time of the motor was set to be 0.3s and 0.5s for rotation and linear translation respectively, the magnitudes are manually defined in the discretization process. Finally, the state-action pairs are collected and

sent to the discriminator D_w. After each rollout, the initial positions of the catheter tip are reset manually, illustrated as the colored bands in the aortic models (Fig. 2(a)). The initial catheter tip position is chosen randomly, aiming to explore more different states in the training. Virtual boundary planes were created inside the 3D model of the aortic arch at 5mm above the origin of the BCA, set as the target of the cannulation. The models are saved after 10 consecutive completions of cannulation to the BCA. There is a limit for each rollout, which is 40 steps for the BCA cannulation.

Fig. 2(a) shows the policy training strategy of the proposed work. The policy for BCA cannulation is then used to cannulate LCCA, an optimization step is performed to ensure higher success rates. This is done by a following RL training phase using PPO, the reward function is manually defined as:

$$r(t) = -k_1 \hat{\mathbf{n}} \cdot ||x_t - x_i|| + k_2 e^{-\hat{\mathbf{n}} \cdot ||x_t - x_i||} \quad (2)$$

where $\hat{\mathbf{n}}$ is the normal vector to the boundary plane where x_i is an index point on the plane. k_1 and k_2 are the weights of the reward function. In this work, they are 1 and 0.5 respectively based on empirical selection. The exponential part of the rewards function encourages faster training. The relative position of the state is set to be the origin of the LCCA (Fig. 2(b)). The training terminates after 10 consecutive successes. The time limit for the cannulation is 60 steps, longer than BCA policy training due to longer procedure length in practice. The architecture for GAIL and PPO training is shown in Fig. 4.

C. Success Rate Test

The success rates of the generated policy were evaluated at first. In this project, the skills of selective catheterization are transferred to cannulate the same blood vessels in a Type-II aortic arch phantom (ElastratSarl, Switzerland). The aortic arch can be classified based on the position of its major branches, with a Type-II arch requiring a more tortuous path to be negotiated in order to catheterize its branches, and therefore presenting the operator with a greater technical challenge when compared to a Type-I arch [22]. One catheter (Beacon Tip 5 Fr VanSchie2, Cook Medical, Bloomington, IN) was used with the Type-I arch cases, and one with a different tip shape (Impress 5 Fr Headhunter1, Merit Medical, South Jordan, UT) for the Type-II arch case, as these were considered the most appropriate choices by our expert clinical advisor. Catheter shapes are shown in Fig. 2(b). The polices learned from Type-I were applied to Type-II arches with no changes. The success rate experiment is designed to test at different initial position/orientation of the tip of catheters. Due to the space constraints in the phantom and the tool limitation, the initial positions/orientations are simplified as four different levels at the ascending aorta with three different tip orientations at each level. The spacing between each level is 5mm. For each initial position/orientation, there are three runs of automated cannulation. The starting levels are shown as colored bands in Fig. 2(b) whereas the initial orientations of the catheter tips are shown in Fig. 2(c). A total of 36 cannulations were executed for each blood vessel, considered successful if the tip of the catheter passed the boundary planes mentioned in the previous section. The time limits for BCA and LCCA are 60 and 80 steps respectively. The proposed GAIL/PPO approaches performed the cannulation of the BCA and the LCCA in both the Type-I and the Type-II aortic arches.

D. User Study Design

To evaluate the performance of the proposed automated robotic framework, a study was carried out to compare with manual catheterization, and robotic teleoperation. Three vascular surgeons were recruited as operators, all of whom had performed more than 300 endovascular procedures but had no formal training in robotic endovascular intervention. In addition, one medical student, with no formal training in vascular procedures, participated. Each operator was asked to perform catheterization of the BCA and LCCA in the Type-I aortic arch phantom, and of the BCA in a Type-II aortic arch phantom. The phantoms were connected to a pulsatile pump to simulate normal human blood flow and optimize the level of realism for tool-tissue interactions. To simulate a real angiography setup, a camera was placed above the phantom, and its live video feed displayed on a monitor in front of the operator. A 6 DoF force sensor was directly placed underneath the vascular phantom (Mini40, ATI) to record forces exerted on the phantom during the catheterization. The root-mean-square forces were calculated from the forces in three dimensions. The setup of the experiment can be seen in Fig. 3. To reduce the effect of a learning curve, the operator was given a familiarization period of 6 min to manipulate the catheter within the setup both manually and with the robot. A single guidewire was used throughout the experiment. For each artery, the operator performed the catheterization maneuver 4 times manually, and 4 times with robotic teleoperation. Prior to commencement of each maneuver, the catheter was placed such that its tip was at a pre-defined band in the ascending aorta (Fig. 2), and the guidewire was advanced through the catheter to provide mechanical support but retracted just far enough to allow the catheter tip to take its shape. The robot with supervised automation activated was then used to catheterize each artery 3 times. For each maneuver, the video feed from the camera and the time taken for the maneuver were recorded. Force-torque sensor readings were recorded at a frequency of 25 Hz. The vascular surgeon who had provided the demonstration training sets for the imitation learning approach was asked to view the recorded videos of the automated catheterizations, and provide qualitative assessment of the maneuvers. Data analysis was performed within each sequence of 4 human-controlled arterial cannulations, the first maneuver was excluded from analysis, to minimize the effect of learning curves. Performance metrics of the catheterization tasks were calculated from the catheter tip motion trajectories, including mean/max tip motion speed, standard deviations of the speed, catheter path length. The Wilcoxon Rank-Sum tests on the metrics were performed.

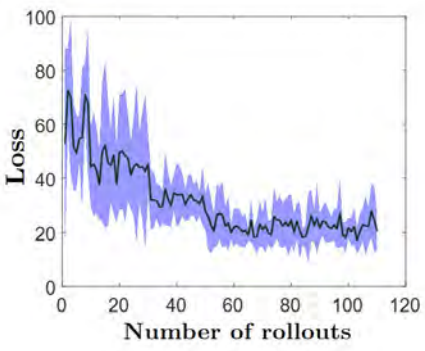

Fig. 5: Loss graph of the proposed GAIL agents training. Bold line is the mean loss and the purple shade is its standard deviation.

TABLE I: Success rate of cannulation of the BCA and LCCA in the Type-I and Type-II aortic arch model with GAIL/PPO policies and Behavior Clone policies

	Type-I Aortic Arch		Type-II Aortic Arch	
	BCA	LCCA	BCA	LCCA
GAIL/PPO	94.4%	88.9%	69.4%	72.2%
Behavior Clone	72.2%	-	5.6%	-

III. Results and Discussion

Table. I shows the results of the success rate test. The proposed learning approach successfully cannulated both the BCA and LCCA in the Type-I aortic arch model in the majority of the trials. Behavior Cloning (BC) policies were trained from the same demonstration data for comparison, it is for BCA cannulation only. The BC approach achieves a higher success rate when cannulating the BCA, the failed cases are mostly due to that the policies are unable to adapt to the difference in orientation while executing rotation. As for the more technically demanding tasks in the Type-II aortic arch model, the proposed GAIL/PPO approaches achieved reasonably high catheterization success rates, and thus demonstrates that the proposed learning methods can adapt to different vascular models. In comparison, the BC approach failed in most trials, the catheter either stuck at the arch or left with its tip incorrectly rotated. Moreover, due to the expensive nature of training in real-world settings as well as hardware limitations, future works include optimizing of the networks taking into account success rates.

Fig. 5 is the loss graph of the proposed GAIL policy training, based on six training with 110 rollouts for each. It shows decreasing mean and standard deviation of the loss function over the number of rollouts. However, fluctuation of the loss was observed, and there is no trend of convergence after 60 rollouts. There are potentially several limitations that may contribute: 1) The robotic driver has different mechanism of manipulating catheter when compared to a human operator, and the hardware may degrade over time; 2) Limited action sets and bang-bang control; 3) Errors in EM tracking sensors such as magnetic interference.

Examples of the catheter tip paths are illustrated in Fig. 6. The proposed automation approach has a similar tip pathway compared to that from expert manual and teleoperation approaches in the Type-I arch for both the BCA and the LCCA. As for the Type-II arch, tip pathways from the proposed approach were similar to those from the expert manual approach. Also, an example catheter tip path from the novice, where manipulation issues during the cannulation can be seen, such as recurrent retractions. Example plots of displacement of the catheter tip against time are also shown. The top right figure depicts the displacement for cannulation of the BCA in the Type-I arch, where the displacement profiles have similar shapes, although in the automated case there is a prolonged initial period of small displacement. The bottom right figure shows displacements of the catheter tip when cannulating the BCA in the Type-II arch. Compared to both the manual and teleoperation cases with the expert surgeon, the automation approach took approximately two times longer. The novice user produced a very different displacement profile, indicating a different behavior due to lack of experience. Those results show that the proposed methods can reasonably imitate the skills of a vascular surgeon.

Table II and Table III present the performance metrics when comparing manual, teleoperation and the proposed automation approaches. In general, lower speed and longer duration of tasks can be seen with the proposed robotic approach. However, with both vascular models, the phantoms were subjected to lower mean and maximum forces with the proposed robotic approach when compared to the manual approach. In clinical practice, lower forces exerted on the arterial walls may imply a lower risk of tissue damage and better clinical outcomes, although there is no generally agreed limit as to a maximum acceptable force. There were higher task duration with the robotic approach, but as interaction forces were less, this cost is outweighed by the benefit of improved overall safety of the procedure; additionally, future works are planned to increase the robot velocities, that potentially improve procedure times while maintaining an acceptable safety profile. Moreover, the standard deviation of the speed is also significantly lower when compared to the expert manual and teleoperation approaches. This is because robot velocities are constant while executing policies. Less variation in speed may lead to lower risk of vessel damage and embolization from instrument manipulation. Furthermore, in the Type-II arch model, large standard deviation (up to 6 times) of total path length can be seen with the expert manual and teleoperation approaches, suggesting less consistent catheter motions across the trials. This highlights the potential benefits of proposed robotic approaches in being consistent and repeatable. Although the number of human participants in this study is small, the data obtained were sufficient to demonstrate significant differences in metrics between the human-controlled and automated approaches.

For qualitative assessment of automated catheterizations, the vascular surgeon who assessed videos of the automated catheterizations noted that, in the successful cases, the selection of movements was generally appropriate and efficient, and there was not a large amount of "overshooting" in the movements. Overall, the movements were noted to be

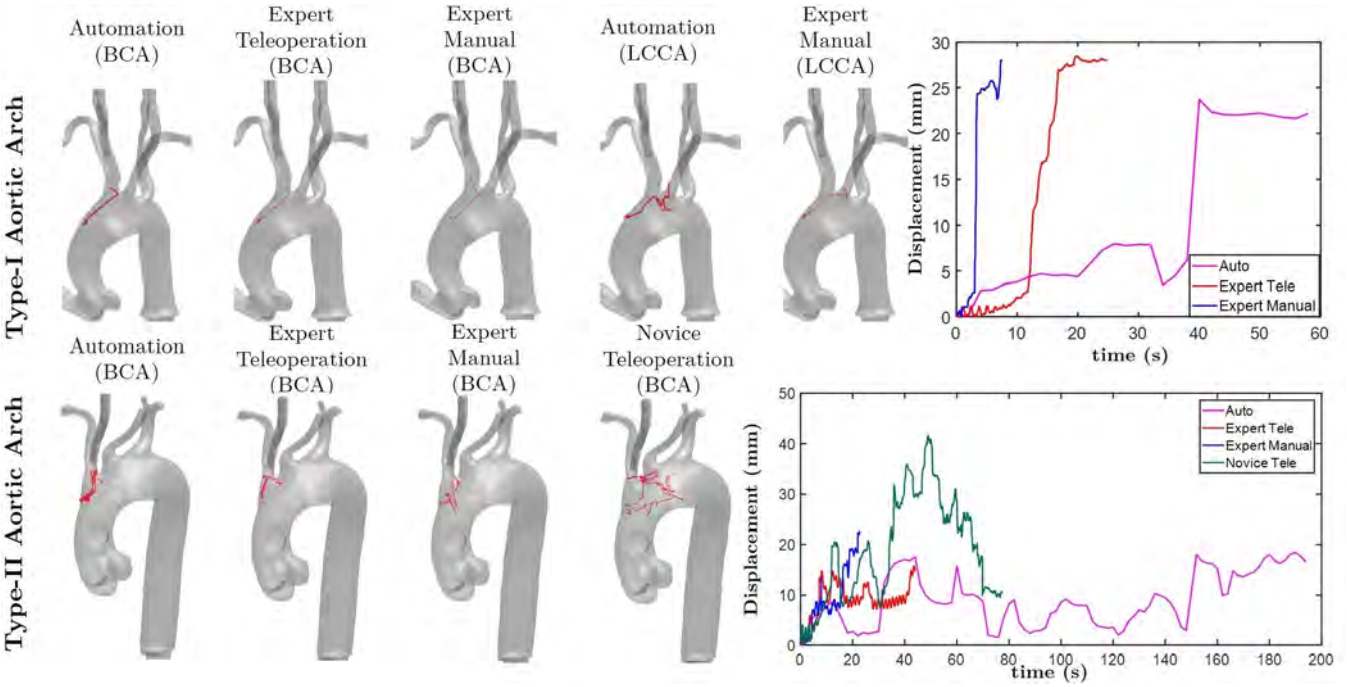

Fig. 6: Examples of catheter tip motion trajectories with different cannulation approaches. Top right: Displacement over time graph for the BCA in the Type-I arch model. Bottom right:Displacement over time graph for the BCA in the Type-II arch model.

TABLE II: Mean value ± std of performance metrics for different cannulation approaches in the Type-I aortic arch

	BCA			LCCA		
	Expert Manual	*Expert Teleoperation	Automation	Expert Manual	*Expert Teleoperation	Automation
Mean force (N)	**1.13±0.56**	0.58±0.11	0.34±0.07	0.78±0.13	0.55±0.09	0.51±0.26
Maximum force (N)	**2.61±0.96**	**1.49±0.22**	0.76±0.12	**2.04±0.53**	1.48±0.67	1.12±0.35
Mean speed (mm/s)	**8.32±1.9**	**3.29±0.23**	1.03±0.03	**8.25±1.6**	**3.09±0.28**	1.39±0.09
STDEV speed (mm/s)	**26.5±7.4**	**9.03±1.8**	1.37±0.23	**22.0±4.0**	**7.59±3.8**	1.22±0.18
Path length (mm)	51.4±8.3	105.0±27.0	55.7±9.4	81.7±29.7	76.3±16.2	106.1±28.7
Procedure Duration (s)	**6.36±1.4**	32.1±9.1	52.1±9.9	**9.85±2.6**	**25.0±6.7**	76.5±24.1

*Missing one user data; **Bold** represents statistically significant results comparing to the automation approach (p<0.05)

TABLE III: Mean value ± std of performance metrics for different cannulation approaches in the Type-II aortic arch

	BCA		
	Expert Manual	Expert Tele.	Automation
Mean force (N)	**0.65±0.27**	**0.49±0.32**	0.18±0.02
Maximum force (N)	**1.95±0.83**	**1.56±1.9**	0.65±0.15
Mean speed (mm/s)	**9.83±2.5**	**6.00±0.71**	1.16±0.26
STDEV speed (mm/s)	**27.6±8.7**	**12.1±4.2**	0.91±0.22
Path length (mm)	184.8±116.2	408.2±302.9	201.6±45.5
Procedure Duration (s)	**17.5±7.1**	**68.7±54.1**	172.3±18.0

Bold represents statistically significant results (p<0.05); "Tele." is the abbreviation of "Teleoperation"

quite slow. In some instances, inappropriate moves were made, seemingly due to real-time position sensing only being available for the tip of the catheter and not other parts of it. Finally, in unsuccessful cases, less adequate behaviors were noted, such advancement of the catheter when its tip was already beyond the target artery, or continuation of withdrawal when the tip was already short of it. Further improvements on the frameworks must include tracking of the entire catheter body.

IV. Conclusion and Future Work

This work proposes a semi-automated framework for robot-assisted endovascular catheterization. Imitation learning is used to extract underlying skill patterns from expert demonstration when performing selective catheterization tasks. Experiments show high success rates with different catheters and vascular models. User studies were conducted with the proposed approach, manual catheterization and robotic teleoperation. The results show fewer interaction forces, more controlled catheter motions, and more consistent catheter paths compared to the manual approach. These suggest less damage to the tissue, and reduced chance of complications. Future works include tracking the entire bodies of the catheter and the guidewire through imaging [23], integration of automated guidewire movements and more complicated catheter actions, as well as prior software simulation for fine-tuning hyperparameters. The proposed framework can be transferred to different catheterization tasks, different vasculature and instruments. The learned tasks and skills can potentially pave the way to next-generation, versatile robot-assisted catheterization platforms.

REFERENCES

[1] S-L Lee, M Constantinescu, W Chi, G-Z Yang, "Devices for Endovascular Interventions: technical advances and translational challenges". NIHR white paper, 2017.

[2] Hausegger KA, Schedlbauer P, Deutschmann HA, and Tiesenhausen K (2001) "Complications in endoluminal repair of abdominal aortic aneurysms". Eur J Radiol 39:22-33. https://doi.org/10.1016/S0720-048X(01)00339-4

[3] C. V. Riga, C. D. Bicknell, A. Rolls, N. J. Cheshire, and M. S. Hamady, "Robot-assisted fenestrated endovascular aneurysm repair (FEVAR) using the Magellan system," J Vasc Interv Radiol, vol. 24, pp. 191-6, Feb 2013.

[4] M. E. M. K. Abdelaziz, D. Kundrat, Marco Pupillo, G. Dagnino, T. M. Y. Kwok, W. Chi, V. Groenhuis, F. J Siepel, C. Riga, S. Stramigioli and G. -Z. Yang, "Toward a Versatile Robotic Platform for Fluoroscopy and MRI-Guided Endovascular Interventions: A Pre-Clinical Study," IROS 2019, pp. 5411-5418.

[5] H.-J. Cha, B.-J Yi, J.Y Won "An assembly-type master-slave catheter and guidewire driving system for vascular intervention" Proceedings of the Institution of Mechanical Engineers, Part H: Journal of Engineering in Medicine Vol 231, Issue 1, pp. 69 - 79, 2016

[6] Z. Q. Feng, G. B. Bian, X. L. Xie, Z. G. Hou and Jian-Long Hao, "Design and evaluation of a bio-inspired robotic hand for percutaneous coronary intervention," 2015 ICRA, Seattle, WA, 2015, pp. 5338-5343.

[7] G.-Z. Yang, J. Cambias, K. Cleary, E. Daimler, J. Drake, P. E. Dupont, et al., "Medical robotics Regulatory, ethical, and legal considerations for increasing levels of autonomy," Science Robotics, vol. 2, pp.8638, 2017.

[8] M. Yip and N. Das,"Robot autonomy for surgery", The Encyclopedia of Medical Robotics. October 2018, pp.281-313.

[9] A. Al Nooryani and W. Aboushokka, "Rotate-on-Retract Procedural Automation for Robotic-Assisted Percutaneous Coronary Intervention: First Clinical Experience," Case Reports in Cardiology, vol. 2018, p. 3, 2018.

[10] Adeline Schwein, Benjamin Kramer, Ponraj Chinnadurai, Neha Virmani, Sean Walker, Marcia O'Malley, Alan B. Lumsden, Jean Bismuth, "Electromagnetic tracking of flexible robotic catheters enables "assisted navigation" and brings automation to endovascular navigation in an in vitro study",Journal of Vascular Surgery, Volume 67, Issue 4, 2018, Pages 1274-1281, ISSN 0741-5214,

[11] H. Rafii-Tari, J. Liu, S.-L. Lee, C. Bicknell, and G.-Z. Yang, "Learning-Based Modeling of Endovascular Navigation for Collaborative Robotic Catheterization," MICCAI, 2013, pp. 369-377.

[12] W. Chi, J. Liu, H. Rafii-Tari, C. Riga, C. Bicknell, and G.-Z. Yang, "A learning based Learning-based endovascular navigation through the use of non-rigid registration for collaborative robotic catheterization" Int. J. Computer Assisted Radiology and Surgery 13(6): 855-864 (2018)

[13] W. Chi et al., "Trajectory Optimization of Robot-Assisted Endovascular Catheterization with Reinforcement Learning," IROS 2018, pp. 3875-3881.

[14] D. Silver et al., "Mastering the game of go without human knowledge," Nature, vol. 550, no. 7676, pp. 354-359, 2017.

[15] J. Ho and S. Ermon, "Generative adversarial imitation learning," in Proc. Adv. Neural Inf. Process. Syst. Conf., 2016, pp. 4565-4573.

[16] L. Tai, J. Zhang, M. Liu and W. Burgard, "Socially Compliant Navigation Through Raw Depth Inputs with Generative Adversarial Imitation Learning," ICRA 2018 pp. 1111-1117.

[17] J. Tan et al., "Sim-to-real: Learning agile locomotion for quadruped robots," 2018, arXiv:1804.10332.

[18] C. Finn, S. Levine, and P. Abbeel, "Guided cost learning: Deep inverse optimal control via policy optimization," in Proc. Int. Conf. Mach. Learn., 2016, pp. 49-58

[19] X. Tan, C. Chng, Y. Su, K. Lim and C. Chui, "Robot-Assisted Training in Laparoscopy Using Deep Reinforcement Learning," in IEEE Robotics and Automation Letters, vol. 4, no. 2, pp. 485-492, April 2019.

[20] B. D. Ziebart, A. L. Maas, J. A. Bagnell, and A. K. Dey, "Maximum entropy inverse reinforcement learning," in 23rd AAAI Conf. Artif. Intell., Chicago, IL, USA, 2008, vol. 8, pp. 1433 1438.

[21]] J. Schulman, F. Wolski, P. Dhariwal, A. Radford, and O. Klimov, "Proximal policy optimization algorithms," 2017, arXiv:1707.06347.

[22] Hicks CW, Malas MB. Cerebrovascular disease: carotid artery stenting. In: Sidawy AN, Perler BA, editors. Rutherford's vascular surgery and endovascular therapy. 9th ed. Philadelphia: Elsevier; 2019:1215-33.

[23] A. Nguyen, D. Kundrat, G. Dagnino, W. Chi, M. E. M. K. Abdelaziz, Y. Ma, T. M. Y. Kwok, C. Riga and G. -Z. Yang,"End-to-End Real-time Catheter Segmentation with Optical Flow-Guided Warping during Endovascular Intervention," ICRA 2020.